CrystEngComm

Probing Hydrogen and Halogen-Oxo Interactions in Uranyl Coordination Polymers: A Combined Crystallographic and Computational Study

Journal:	*CrystEngComm*
Manuscript ID	CE-ART-04-2018-000682.R1
Article Type:	Paper
Date Submitted by the Author:	01-Jun-2018
Complete List of Authors:	Carter, Korey; E O Lawrence Berkeley National Laboratory, Chemical Sciences Kalaj, Mark; The George Washington University, Chemistry Kerridge, Andrew; Lancaster University, Chemistry Cahill, Chris; The George Washington University, Chemistry

Probing Hydrogen and Halogen-Oxo Interactions in Uranyl Coordination Polymers: A Combined Crystallographic and Computational Study

Korey P. Carter[§], Mark Kalaj[§], Andrew Kerridge[∞], and Christopher L. Cahill*[§]
§ Department of Chemistry, The George Washington University, 800 22nd Street, NW, Washington, D.C. 20052, United States
∞ Department of Chemistry, Lancaster University, Bailrigg, Lancaster LA1 4YB, United Kingdom

Abstract

The syntheses and crystal structures of four compounds containing the UO_2^{2+} cation and either benzoic acid (**1**), *m*-chlorobenzoic acid (**2**), *m*-bromobenzoic acid (**3**), or *m*-iodobenzoic acid (**4**) are described and the vibrational spectroscopic properties for compounds **3** and **4** are reported. Single crystal X-ray diffraction analysis of these materials shows that uranyl oxo atoms are engaged in non-covalent assembly via either hydrogen (**1** and **2**) or halogen bonding (**3** and **4**) interactions. The halogen bonding in compounds **3** and **4** is notable as the crystallographic metric percentage of the sum of the van der Waals radii indicates these interactions are of similar strength. Characteristics of the halogen-oxo interactions of **3** and **4** were probed via Raman and Infrared spectroscopy however, which revealed significant differences in stretching frequency values for the two compounds. Additionally, compounds **3** and **4** were characterized via quantum chemical calculations and density-based quantum theory of atoms in molecules (QTAIM) analysis, which indicated that the I-oxo interaction in **4** is likely the stronger of the two interactions, with differences between the two interactions resulting from both inductive effects and halogen polarizability.

Introduction

Crystal engineering within actinide hybrid materials, in particular those incorporating hexavalent uranium, is an area of sustained interest as it has proven to be a route that allows for the rational preparation of materials with desired structures and properties.[1-11] This approach is predicated upon the directed assembly of tectons into crystalline architectures via attractive, noncovalent synthons, and utilization within uranyl hybrid materials has necessitated the development of a hierarchy of acceptor-donor pairing preferences based on a detailed knowledge of the relationship between intra- and intermolecular interactions.[12] Recently, our group has been investigating the potential for crystal engineering to support engagement of the nominally terminal uranyl oxo groups,[13-17] and here we continue these efforts, employing hydrogen and halogen bonding for assembly and then describing uranyl oxo atom behavior as a synthon acceptor site. Development of a hierarchy of uranyl acceptor-donor pairing preferences requires a metric for adjudicating interaction strengths, which can then be qualitatively applied to judging which synthon acceptor and donor sites are 'best'. Within solid-state materials, the percentage of the sum of the van der Waals radii is commonly utilized to quantify interaction strengths,[18, 19] yet this metric has its limitations,[20, 21] as demonstrated recently when sum of the vdW radii identified a Cl•••Oxo interaction that electrostatic surface potentials definitively showed was a mere consequence of packing.[16]

Herein we expand our efforts in this arena and use four uranyl hybrid materials (two novel and two known) that feature benzoic acid ligands with systematically varied *meta*-substituents (benzoic acid (**1**), *m*-chloro- (**2**), *m*-bromo- (**3**), and *m*-iodobenzoic acid (**4**)) to probe the value and limits of this crystallographic metric. Uranyl oxo atom

participation in bonding via 'oxo-functionalization' is a growing area of research,[22-26] whereas oxo engagement in hydrogen and halogen bonding synthons remains underexplored,[6, 27] particularly within simple coordination chemistry, with successful efforts often requiring a dual ligand strategy wherein strongly electron donating N-donor ligands in the equatorial plane are paired with benzoic acid linkers featuring polarizable halogen atoms at their periphery to facilitate halogen bonding interactions.[14, 16] Compounds **1**-**4** all *lack* an equatorial electron donating species, yet feature either hydrogen or halogen bonding with the uranyl oxo atoms, and the syntheses, crystal structures, and modes of supramolecular assembly are reported for all four materials. Of particular note are compounds **3** and **4**, which both feature halogen bonding interactions at the uranyl oxo atoms. Crystallographic metrics, i.e. the percentage of the sum of the van der Waals radii, indicate these interactions are equivalent, yet we extend our investigation into (relative) interaction strengths beyond the structural lens by also characterizing **3** and **4** via spectroscopic and computational means. Vibrational spectra (Raman and Infrared spectroscopy) revealed **4** is redshifted with respect to **3**, which corresponded with an increase in halogen polarizability between the two materials, whereas quantum chemical calculations at the density functional (DFT) level of theory along with density-based quantum theory of atoms in molecules (QTAIM) analysis highlighted that differences in interaction strength, which are observed in vibrational spectra, are partially due (ca. 50%) to electronic differences in the equatorial ligands, with the other ca. 50% of the observed shift resulting from changing halogen polarizability.

Experimental Section

Materials and Methods

Caution: Whereas the uranium oxyacetate dihydrate $[UO_2(CH_3COO)_2]\bullet 2H_2O$ and uranyl nitrate hexahydrate $[UO_2(NO_3)_2]\bullet 6H_2O$ used in this study consists of depleted uranium, standard precautions for handling radioactive and toxic substances should be followed.

All organic materials, benzoic acid (Sigma Aldrich, ≥99.5%), *m*-chlorobenzoic acid (Alfa Aesar, 99%), *m*-bromobenzoic acid (Alfa Aesar, 98+%), and *m*-iodobenzoic acid (Alfa Aesar, 98+%), were purchased and used as received.

Synthesis

All compounds discussed herein were synthesized via hydrothermal methods at autogenous pressure in a 23 mL Teflon-lined Parr bomb at an oven temperature of 150 ˚C for 48 hours. A molar ratio of (1:2:667-UO_2^{2+}-benzoic acid-water) was used for compounds **1**-**4**. Upon removal from the oven, the samples were allowed to cool to ambient temperature over four hours and then opened after approximately twelve hours. Yellow plate like crystals were obtained from the bulk product after removing the supernatant liquor, washing with distilled water and ethanol, and air-drying at room temperature.

Characterization

X-Ray Structure Determination

Single crystals from each bulk sample were isolated and mounted on MiTeGen micromounts. Structure determination for each of the single crystals was achieved by collecting reflections using 0.5˚ ω scans on a Bruker SMART diffractometer equipped with an APEX II CCD detector using MoKα (λ=0.71073 Å) radiation at 293(2) K. The

data were integrated using the SAINT[28] software package contained within the APEX II software suite,[29] and an absorption correction was performed for compound **3** using *SADABS*.[30] The crystals selected from the bulk product of compounds **1**, **2**, and **4** were two component non-merohedral twins and were treated accordingly using *TWINABS*.[31] Compounds **1-4** were solved via direct methods using SIR 92.[32] All four compounds were refined using SHELXL-2014[33] contained within the WinGX[34] software suite. In each structure, all non-hydrogen atoms were located via difference Fourier maps and refined anisotropically. Aromatic hydrogen atoms were located via difference Fourier maps, yet were placed at their idealized positions and allowed to ride on the coordinates of their parent carbon atom ((U_{iso}) fixed at $1.2U_{eq}$). All figures were prepared with CrystalMaker.[35] Data collection and refinement details for compounds **1-4** are included in Table 1.

Table 1 Crystallographic Data for Compounds **1-4**

	1	**2**	**3**	**4**
chem formula	$C_{14}H_{10}O_6U$	$C_{28}H_{20}Cl_4O_{14}U_2$	$C_{14}H_8Br_2O_6U$	$C_{14}H_8I_2O_6U$
formula weight	512.25	1198.30	670.05	764.03
crystal system	monoclinic	monoclinic	monoclinic	monoclinic
space group	*C*2/m	$P2_1$/c	$P2_1$/c	$P2_1$/c
a (Å)	7.632(6)	18.391(8)	5.1074(4)	5.0806(4)
b (Å)	17.468(9)	8.604(5)	17.6516(15)	17.9621(12)
c (Å)	5.313(5)	10.512(7)	9.0688(8)	9.3867(6)
α (deg)	90	90	90	90
β (deg)	95.791(7)	90.911(6)	94.061(6)	93.553(8)

γ (deg)	90	90	90	90
V (Å^3)	704.7(9)	1663.2(16)	815.53(12)	854.97(10)
Z	2	2	2	2
T (K)	293(2)	293(2)	293(2)	293(2)
λ (Mo Kα)	0.71073	0.71073	0.71073	0.71073
D_{calc} (g cm^{-3})	2.414	2.393	2.729	2.968
μ (mm^{-1})	11.540	10.113	14.876	13.128
R_{int}	0.0415	0.0396	0.0326	0.0281
R1 [I>2σ(I)]	0.0141	0.0246	0.0223	0.0233
wR2 [I>2σ(I)]	0.0322	0.0580	0.0512	0.0570

Powder X-ray Diffraction

Powder X-ray diffraction (PXRD) data on the bulk reaction product of compounds **1-4** (Figures S4-S7, Supporting Information) were used to examine the purity of typical preparations. All data were collected on a Rigaku Miniflex (Cu Kα, 2θ=3-60˚) and were analyzed using the JADE software program.[36] Initially, the bulk products of **1-3** contained multiple phases. The bulk samples of **1** and **3** were purified by decreasing the solution concentration (adding more solvent) and shortening the reaction time, respectively. Attempts were made to identify and/or remove the impurities from **2** by using a range of organic solvents and reaction conditions, yet they persisted and thus prevented further characterization of this material.

Spectroscopic Characterization

Infrared spectra of single crystals of **3** and **4** were collected from 400 to 4000 cm^{-1} using a Bruker Tensor 27 FT-IR microspectrometer. Crystals were placed on glass microscope slides and crushed using a diamond attenuated total reflectance (ATR) microscope objective. Raman spectra for single crystals of **3** and **4** were collected using a Bruker Sentinel system linked via fiber optics to a video assisted Raman probe equipped with a 785 nm 400 mW and a high sensitivity TE-cooled, 1024 x 255 CCD array. The spectra were collected for 15 seconds with four signal accumulations over the range of 80-3200 cm^{-1}. For both IR and Raman, spectra were collected in triplicate with the average of the three IR and Raman spectra for each compound reported as the corresponding final spectrum.

Room temperature solid-state luminescence measurements were obtained for **3** and **4** on a Horiba JobinYvon Fluorolog-3 spectrophotometer and data were manipulated using the FluoroEssence software package. Samples were prepared by gently grinding approximately twenty milligrams of material with a mortar and pestle. Approximately eight drops of cyclohexane were added and the resulting slurry was then added dropwise to a microscope slide with drops focused on a targeted area in order to increase the sample concentration and enhance the resulting luminescence spectra. The solid material was allowed to air dry for approximately ten minutes, allowing for the evaporation of cyclohexane before a cover slide was placed on top of the sample and secured with adhesive tape.

Computational Details

Density functional theory (DFT) calculations have been performed using version 6.4 of the TURBOMOLE quantum chemistry software package.[37] Ahlrichs def2-TZVP basis sets of triple-zeta quality have been used for the C, H, O, and U atoms,[38] with the basis set for U incorporating a relativistic ECP comprising 60 core electrons.[39] All simulations were performed using the B3LYP hybrid-GGA exchange-correlation functional, which has been to shown to reproduce experimental parameters of uranyl complexes with high accuracy.[40, 41] To maintain a realistic coordination environment for uranyl cations, only the geometries of the uranyl unit, coordinating species (4 × O, 2 × X), and O-terminating hydrogens were optimized. Analysis of resultant electron densities was performed using Bader's Quantum Theory of Atoms in Molecules (QTAIM) approach[42] via version 13.11.04 of the AIMA11 software suite.[43]

Results

Description of Structures

Single crystal X-ray crystallography analyses revealed three unique coordination environments in this family of uranyl hybrid materials. Compounds **1**, **3**, and **4** (with benzoic acid, *m*-bromo-, and *m*-iodobenzoic acid) are 1D coordination polymers constructed from monomeric SBUs, whereas compound **2** (with *m*-chlorobenzoic acid) is a molecular dimer featuring one crystallographically unique UO_2^{2+} cation. Local structures are briefly described for compounds **1**, **2**, and **4** as they represent each of the unique coordination environments. Modes of supramolecular assembly are described for all compounds as they are affected by systematic changes in the functional groups at the periphery of the benzoic acid ligands.

Single crystal X-ray diffraction analysis reveals that compound **1**, $[UO_2(C_7H_5O_2)]_n$, crystallizes in the monoclinic space group C2/m, and although the structure of **1** has been reported previously,[44] it is included here for context and comparison. Compound **1** features a single crystallographically unique uranyl cation that has adopted square bipyramidal coordination geometry. Each uranyl cation is coordinated by two axial oxygen atoms (O1 and O1') and four equatorial oxygen atoms (O2 and O2') from bridging bidentate benzoic acid ligands (Figure 1). U1-O2 distances to the bridging bidentate benzoic acid ligand (O2, O2') are 2.297(2) Å. The square bipyramidal uranyl centers are connected by the bridging bidentate benzoic acid groups to form 1D chains that propagate in the [001] direction. The 1D chains of **1** are linked to form a 2D sheet in the (100) plane via weak hydrogen bonding (C-H•••O) interactions between the uranyl oxo atom (O1) and an aromatic hydrogen atom (H4) at a distance of 2.72 Å (Figure 1), and whereas weak C-H•••O hydrogen bonding interactions with the uranyl oxo atoms are relatively common,[22, 45] this is the *only* example of this synthon we observe in this family of compounds.

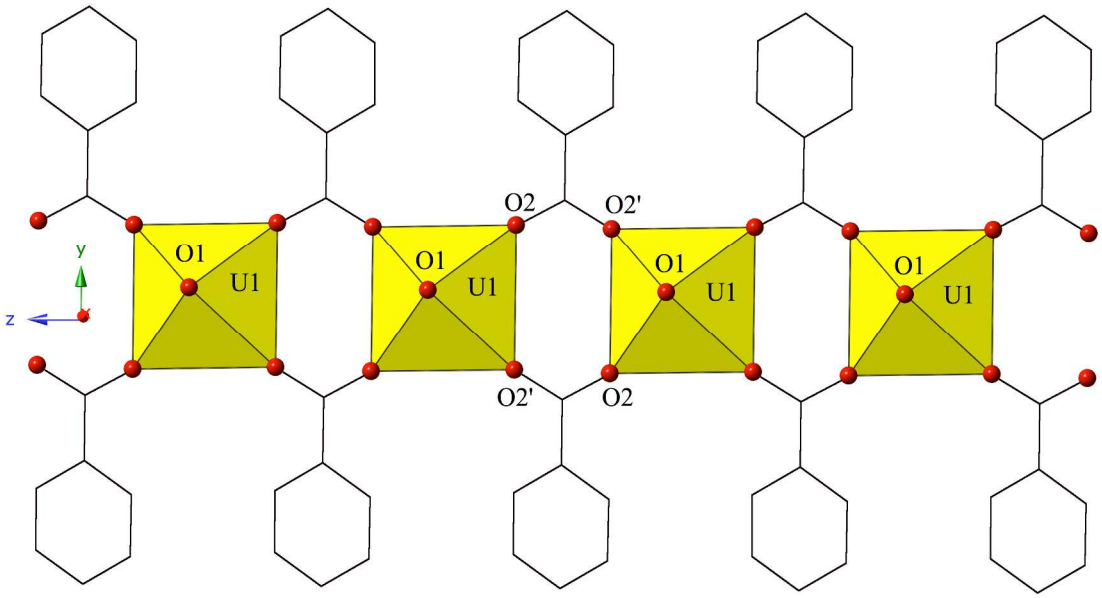

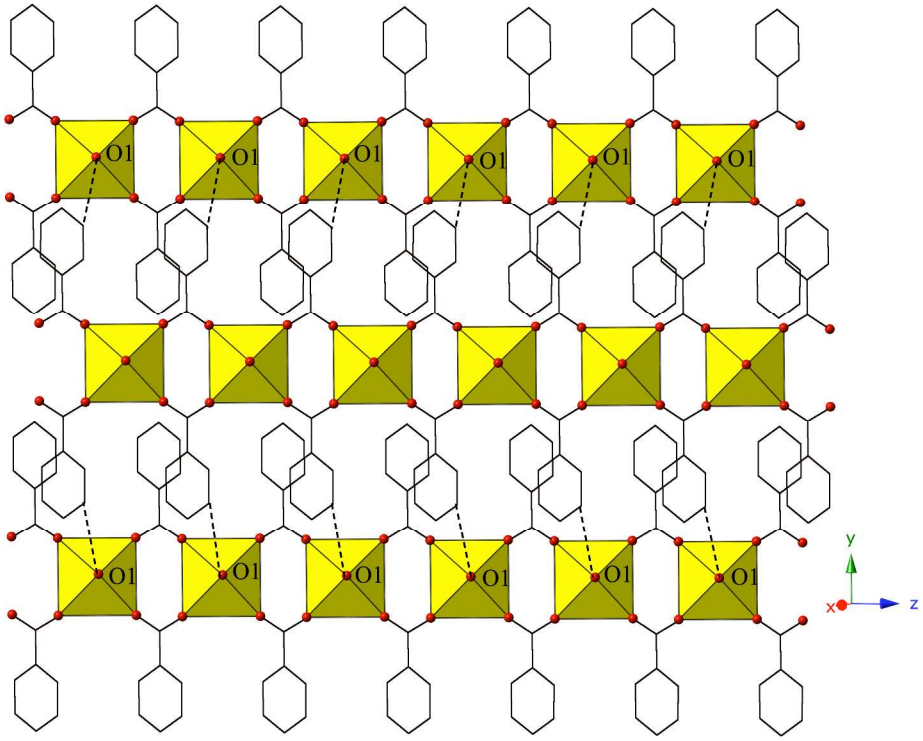

Figure 1 (Top) Polyhedral representation of compound **1**. Yellow polyhedra are U(VI) centers, whereas spheres represent oxygen atoms (red). (**Bottom**) **1** viewed in the (100) plane highlighting C-H•••O hydrogen bonding interactions with uranyl oxo atoms that assemble chains of **1** into a supramolecular 2D sheet.

Compound **2**, $[UO_2(C_7H_4ClO_2)_2(H_2O)]_2$, crystallizes in the space group $P2_1/c$ and features a local structure that contains a uranyl dimer where a unique $[UO_2]^{2+}$ cation and its symmetry equivalent have each adopted pentagonal bipyramidal coordination geometries (Figure 2). The crystallographically unique $[UO_2]^{2+}$ cation is chelated by a bidentate *m*-chlorobenzoic acid ligand and U1-O bond distances (O3 and O4) are 2.391(3) Å (U1-O3) and 2.446 (3) Å (U1-O4), respectively. Linking the uranyl cation and its symmetry equivalent is a bridging bidentate *m*-chlorobenzoic acid ligand (O5 and O6) and U1-O bond lengths to both oxygen atoms are 2.328(3) Å. Completing the equatorial coordination sphere of the uranyl cation is a bound water molecule (OW1) at a distance of 2.477(3) Å, which facilitates intermolecular, bifurcated hydrogen-bonding

interactions with uranyl oxo atoms O1 and O2 (Figure 2). The uranyl tectons of **2** are assembled into infinite 1D chains that propagate in approximately the [010] direction via O-H•••O hydrogen bonding, and interaction distances from the hydrogen atoms on OW1 are 2.70(6) Å (HW1-O1) and 1.94(4) Å (HW2-O2), respectively.

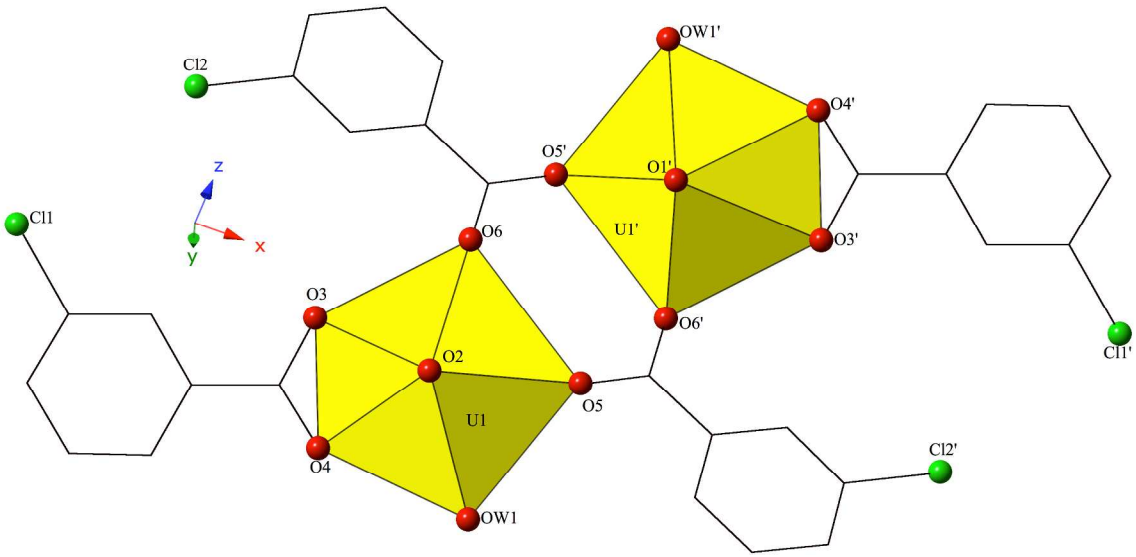

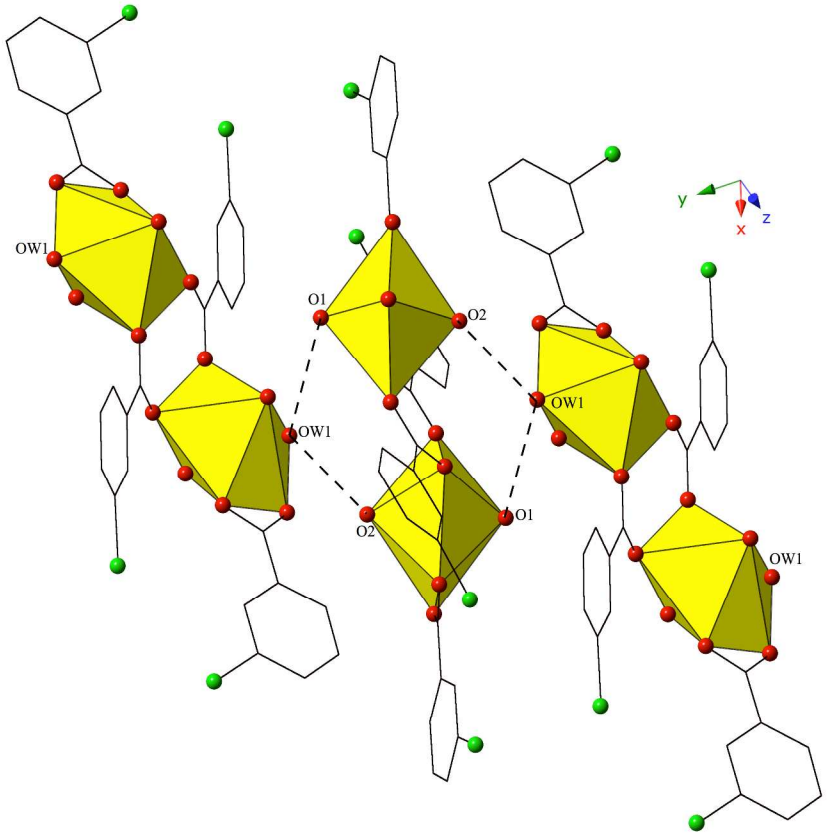

Figure 2 (Top) Polyhedral representation of compound **2**. Green spheres represent chlorine atoms. (**Bottom**) **2** viewed along approximately the [010] direction illustrating the bifurcated O-H•••O hydrogen bonding interactions that link dimers of **2** into a 1D chain.

Single crystal X-ray diffraction analysis reveals that compounds **3** $[UO_2(C_7H_4BrO_2)]_n$ and **4** $[UO_2(C_7H_4IO_2)]_n$ are isomorphous and crystallize in the monoclinic space group $P2_1/c$. As such only compound **4** will be described here as the structure of **3** has been reported previously.[46] The asymmetric unit of **4** is very similar to **1** and features a single crystallographically unique uranyl cation, which has adopted square bipyramidal coordination geometry. Each $[UO_2]^{2+}$ cation is coordinated by six oxygen atoms, the two axial oxygen atoms (O1 and O1') of the uranyl unit and four oxygen atoms (O2, O2', O3, and O3') from bridging bidentate *m*-iodobenzoic acid ligands (Figure 3). U1-O bond distances to the bridging bidentate *m*-iodobenzoic acid

ligand (O2 and O3) are 2.316(3) Å and 2.288(3) Å, respectively, and the iodine atom (I1) of the *m*-iodobenzoic acid ligand facilitates intermolecular I-O interactions that will be discussed further in the next paragraph. The square bipyramidal uranyl centers are connected by the bridging bidentate benzoic acid groups to form 1D chains that propagate in the [100] direction (Figure 3).

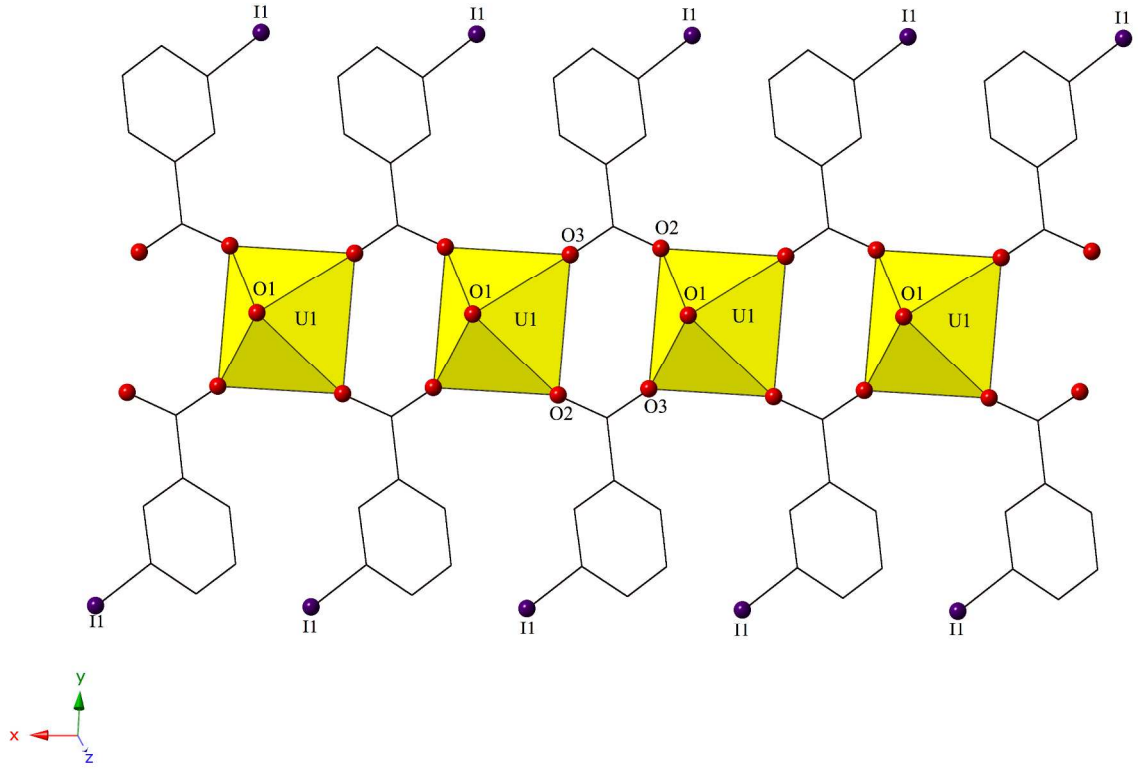

Figure 3 Polyhedral representation of compound **4**. Purple spheres represent iodine atoms.

The 1D chains of **4** are linked to form a supramolecular 2D sheet in the (010) plane via halogen bonding interactions between the iodine atoms from the *m*-iodobenzoic acid ligands (I1) on one chain with the axial uranyl oxygen atoms (O1) on each uranyl metal center of an adjacent 1D chain (Figure 4). These oxo interactions differ from those

in **2** owing to the participation of the iodine (halogen bonding) instead of the hydrogen bonded water molecule. The corresponding I-O interaction distance and angle are 3.319(4) Å (94.8% sum of the van der Waals radii) and ∠C4-I1-O1 (160.20º). Similar to **4**, the 1D chains of **3** are also linked to form a supramolecular 2D sheet in the (010) plane via halogen bonding interactions between the bromine atoms of the *m*-bromobenzoic acid ligands (Br1) on one chain with the axial uranyl oxygen atoms (O1) on each uranyl metal center of the adjacent chain (Figure S1, Supporting Information). The corresponding Br-O interaction distance and angle are 3.193(4) Å (94.7 % sum of the van der Waals radii) and ∠C4-Br1-O1 (161.83°).

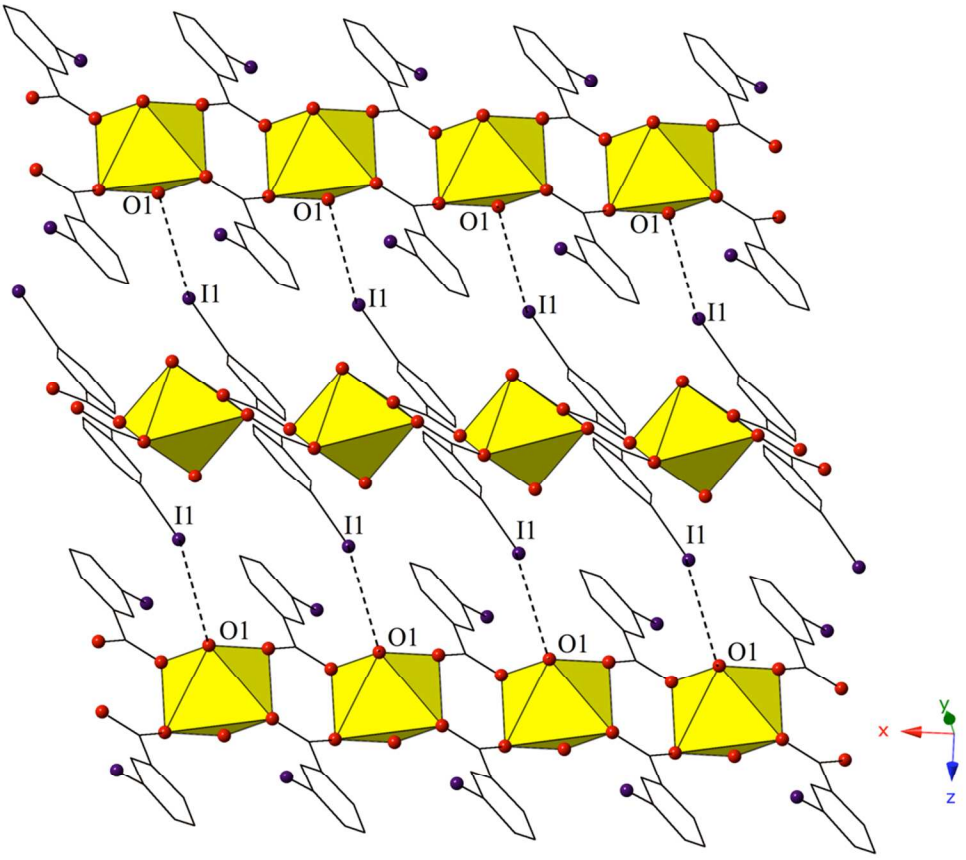

Figure 4 Compound **4** viewed in the (010) plane highlighting I-O halogen-oxo interactions that assemble chains of **4** into a supramolecular 2D sheet.

Structural Discussion

As the tectons and topologies observed in **1**-**4** have precedent in the extensive catalog of uranyl hybrid materials,[3, 6, 47] we focus our discussion on the modes of supramolecular assembly in these compounds. The supramolecular synthons observed in **1**-**4** all involve the nominally terminal uranyl oxo atoms, which can be engaged for assembly as we have demonstrated in multiple recent studies,[13, 14, 16, 17] yet examples of oxo atoms acting as hydrogen and halogen bonding acceptors in the absence of equatorial chelation by electron rich ligands, as is the case for **1**-**4**, remains uncommon.[15] The 1D chains of **1** are composed of monomeric uranyl building units decorated by benzoic acid ligands and assembly into a supramolecular 2D sheet is the result of weak C-H•••O hydrogen bonding interactions. Replacing benzoic acid with *m*-chlorobenzoic acid yields compound **2** where we observe discrete uranyl dimers linked into 1D chains via O-H•••O hydrogen bonding interactions between the coordinated water molecule and uranyl oxo atoms. This observation reveals that the polarizability of chlorine is likely not sufficient to promote halogen bonding with uranyl oxo atoms, consistent with results from a recent study,[17] while explicitly demonstrating the hierarchy of hydrogen bonding with uranyl oxo atoms (O-H groups are 'better' hydrogen bond donors than C-H groups).

The 1D chains of **3** and **4** are both composed of monomeric uranyl building units, similar to **1**, which are decorated by *m*-bromo- and *m*-iodobenzoic acid ligands, respectively, with assembly into a supramolecular 2D sheet now the result of *halogen*-oxo interactions (Figure 5). These two compounds are isomorphous and the structural similarities extend to halogen bonding strengths, as determined using the crystallographic metric percentage of the sum of the van der Waals radii, with the Br-O interaction in **3**

and the I-O interaction in **4** at 94.7% and 94.8% sum of the van der Waals radii, respectively. As there is an increase in halogen polarizability (Br<I) between **3** and **4**, halogen bond strengths are not expected to be 'identical,' thus highlighting a limitation with our crystallographic efforts to gauge strengths of halogen-oxo interactions.

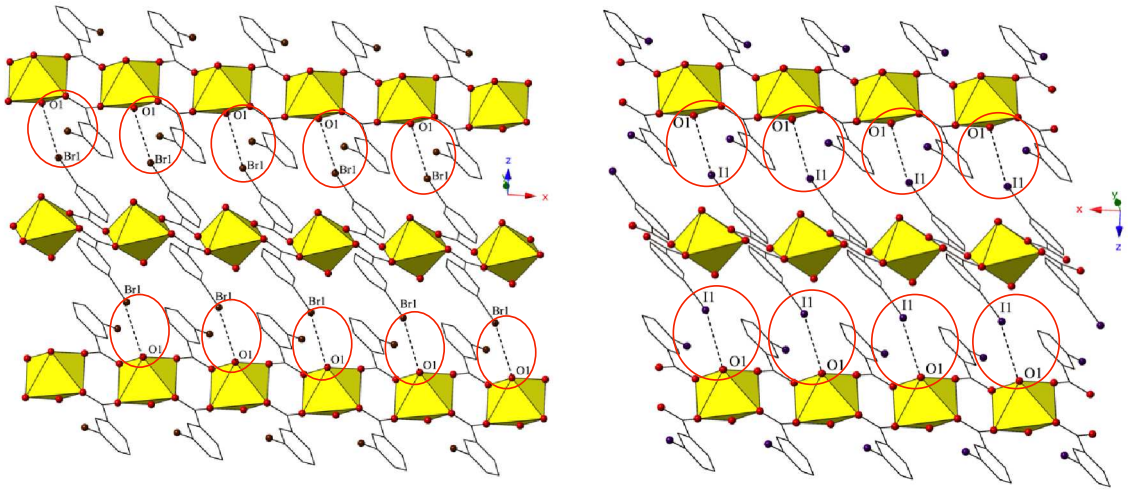

Figure 5 Compounds **3** and **4** with *m*-bromo- (**Left**) and *m*-iodobenzoic acid (**Right**) viewed in the (010) plane illustrating the Br-O and I-O halogen-oxo interactions that assemble chains of **3** and **4** into 2D sheets.

Vibrational Spectroscopy

As the halogen-oxo interactions in compounds **3** and **4** (with *m*-bromo- and *m*-iodobenzoic acid) are of nearly identical strengths according to crystallographic metrics, we turned to Raman and IR spectroscopy to further probe the nature of these interactions. The uranyl cation is known to feature three characteristic vibrational modes: a symmetric stretching mode (ν_1, 860-880 cm^{-1}, Raman active), a bending mode (ν_2, 200-210 cm^{-1}, infrared active), and an asymmetric stretching mode (ν_3, 930-960 cm^{-1}, infrared active),[48-50] and the frequencies of these vibrational modes, in particular ν_1 and ν_3, provide valuable spectroscopic information about relative strengths of U=O bonds (which are affected by halogen-oxo interactions).[16, 17, 27] A look at the Raman and IR spectra of compounds **3**

and **4** reveals redshifts (6 cm^{-1} in the Raman and 11 cm^{-1} in the IR) with respect to the *m*-iodo compound (**4**) when comparing to the *m*-bromo compound (**3**) (Figure 6). These findings qualitatively illustrate that the iodo-oxo interaction in **4** has a *greater* effect on the uranyl oxo group, and also suggest that the oxo interactions in **3** and **4** may not be of 'equivalent strength', as suggested by crystallography.

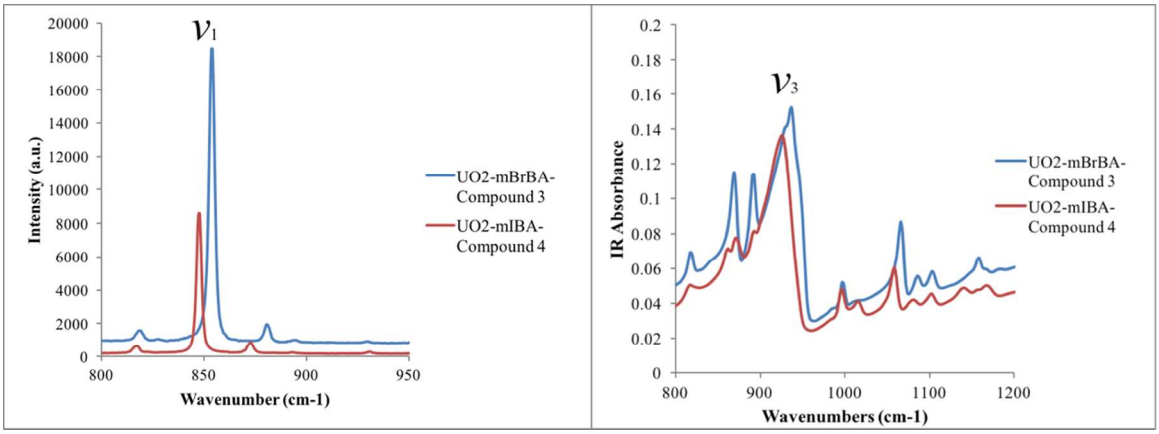

Figure 6 Raman and IR spectra of compounds **3** (blue) and **4** (red) highlighting shifts in the symmetric (ν_1) and asymmetric (ν_3) stretches of the uranyl cation.

Computational Results

In an effort to rationalize structural and spectroscopic findings on the halogen-oxo interactions of compounds **3** and **4**, we turned to density functional theory (DFT) calculations and quantum theory of atoms in molecules (QTAIM) analysis to probe the results highlighted in previous sections. Initial DFT calculations were performed on a model system consisting of a uranyl cation coordinated by six *m*-halobenzoic acid ligands (Hal=Br or I), where all six halobenzoates were protonated to truncate the periodic system (Figure 7). Four *m*-halobenzoic acid ligands coordinate the uranyl cation equatorially via carboxylate oxygen atoms, whereas two moieties bind uranyl oxo atoms via halogen functional groups (Figure 7).

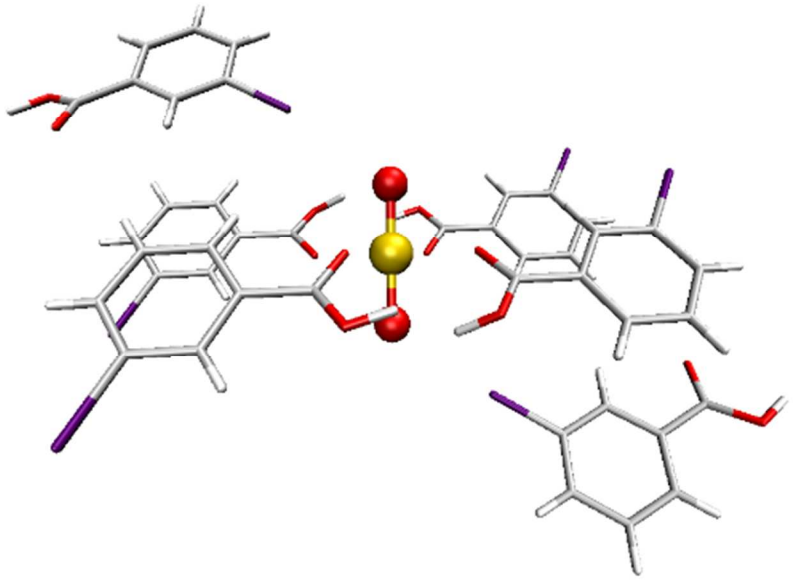

Figure 7 Molecular model of uranyl cation coordinated by six halobenzoic acids (halobenzoates protonated to truncate periodic system). Four ligands coordinate uranium equatorially via oxygen atoms, while two coordinate oxo atoms via halogen functional groups, $[UO_2(C_7H_5XO_2)_6]^{2+}$.

Initial optimizations on the model described in Figure 7 were performed with the PBE and PBE0 functionals. The latter resulted in significantly better agreement with experimental bond lengths, however Hal-oxo bond lengths were overestimated using both functionals. PBE0 structures were therefore reoptimized with dispersion interactions included via Grimme's D3-approach, which led to better agreement with experimental values. To check the validity of the PBE0 data, structures were reoptimized using the B3LYP functional and the D3 dispersion correction. Results of partial optimizations are summarized in Table 2. PBE0- and B3LYP-calculated U-oxo and U-O_{eq} bond lengths were found to be in excellent agreement with experiment, whereas Hal-oxo bond lengths remained slightly overestimated.

Table 2 Comparison of experimental and DFT/def(2)-TZVP optimized bond lengths. Values in parentheses obtained in the absence of dispersion correction. All values are in Å.

	Hal=Br				Hal=I			
	Exp.	**PBE**	**PBE0**	**B3LYP**	**Exp.**	**PBE**	**PBE0**	**B3LYP**
U-oxo	1.743	- (1.790)	1.746 (1.746)	1.767 (-)	1.765	- (1.795)	1.748 (1.748)	1.769 (-)
U-O_{eq}	2.299	- (2.313)	2.311 (2.312)	2.315 (-)	2.302	- (2.316)	2.313 (2.312)	2.314 (-)
Hal-oxo	3.193	- (3.193)	3.212 (3.232)	3.177 (-)	3.319	- (3.375)	3.388 (3.420)	3.352 (-)

To investigate the effect of the Hal-oxo interactions on structural metrics (i.e. bond distances), the groups supporting these interactions were removed (see Figure S2, Supporting Information) and the systems were reoptimized. Table S1 (SI) summarizes the results of these reoptimzations and reveals the structural effect of the Hal-oxo interaction to be minimal. Topological analysis of the PBE0 and B3LYP derived electron densities was also performed using the Quantum Theory of Atoms in Molecules (QTAIM). Hal-oxo bond critical points, indicating (in this case ionic) chemical interactions, were found in all cases, although the magnitude of these interactions are weak (Table 3).

Table 3 Topological parameters of Hal-oxo bond critical points. ρ_{BCP} = magnitude of electron density at bond critical point and H_{BCP} = magnitude of energy density at bond critical point. All values are in a.u.

	Hal=Br		Hal=I	
	PBE0	**B3LYP**	**PBE0**	**B3LYP**
$\boldsymbol{\rho_{\mathrm{BCP}}}$	0.0078	0.0085	0.0074	0.0080
$\boldsymbol{\nabla^2\rho_{\mathrm{BCP}}}$	0.031	0.033	0.026	0.028
$\boldsymbol{H_{\mathrm{BCP}}}$	0.0016	0.0016	0.0014	0.0014

As halogen-oxo interactions were not found to impact uranyl structural metrics in **3** and **4**, consistent with experimental observations from TURBOMOLE, this allowed for vibrational characterization of a subsystem of a complex to be performed. Here the vibrational properties of the uranyl unit, which would be expected to be decoupled from

the coordinating environment, are presented in Table 4. Whereas neither PBE0 nor B3LYP was able to quantitatively simulate the experimental symmetric (Raman-active) and antisymmetric (IR-active) stretch frequencies of uranyl, both were able to provide useful relative values. Considering first the difference in the symmetric stretch values, when the coordinating halide was varied, both PBE0 and B3LYP predict redshifts of 6.2 and 6.3 cm^{-1}, respectively, which is in excellent agreement with an experimental value of 6.0 cm^{-1}. In the absence of Hal-oxo interactions (i.e. using the model shown in Figure S2, Supporting Information), this difference was approximately halved, to 3.0 and 3.4 cm^{-1}, respectively. This demonstrates a small but measurable effect of ~3 cm^{-1} on vibrational frequencies due to Hal-oxo interactions. When considering the asymmetric stretch values, computational and experimental values vary a little with PBE0 and B3LYP predicting (red)shifts of 6.5 and 6.7 cm^{-1}, compared to the 11 cm^{-1} redshift observed experimentally. In the absence of Hal-oxo interactions, using the model from Figure S2, we once again find that ~50% of the calculated difference in stretching frequencies is due to Hal-oxo interactions, consistent with symmetric stretch results described above, with the other ~50% difference in ν_3 values likely a result of subtle, yet important differences in inductive effects between benzoic acid ligands as a function halogen substituent.

Table 4 Vibrational characterization of compounds **3** and **4**. Values in parentheses obtained in absence of Hal-oxo interactions. All values are in cm^{-1}.

	Hal=Br			**Hal=I**			**Δν**		
	Exp.	**PBE0**	**B3LYP**	**Exp.**	**PBE0**	**B3LYP**	**Exp.**	**PBE0**	**B3LYP**
ν(U-oxo)$_{sym}$	853.5	928.2 (927.6)	884.1 (880.8)	847.5	922.0 (924.6)	877.8 (877.4)	6.0	6.2 (3.0)	6.3 (3.4)
ν(U-oxo)$_{asym}$	937	1013.1 (1014.0)	973.1 (971.8)	926	1006.6 (1011.3)	966.4 (968.6)	11.0	6.5 (2.7)	6.7 (3.2)
ν_{asym} - ν_{sym}	83.5	84.9 (86.4)	89.0 (91.0)	78.5	84.6 (86.7)	88.6 (91.2)	-	-	-

Conclusions

The synthesis and crystal structures of four uranyl hybrid materials featuring benzoic acid, *m*-chloro-, *m*-bromo-, and *m*-iodobenzoic acid are reported, their means of supramolecular assembly have been detailed, and vibrational spectra for compounds **3** and **4** have been collected. This family of materials is another example of the uranyl oxo atoms being systematically involved in non-covalent assembly,[14, 16, 17] which continues to demonstrate the feasibility of engaging the nominally terminal oxo atoms via supramolecular means, and these efforts are complementary with ongoing efforts in actinide organometallic chemistry investigating 'oxo-functionalization'.[22-26] As crystallographic metrics suggested the halogen-oxo interactions in **3** and **4** were of equivalent strength, yet vibrational spectra suggested otherwise, density functional calculations and QTAIM analysis were used to probe crystallographic and spectroscopic differences. Computational results indicated that the I-oxo interaction in compound **4** is likely stronger than the Br-oxo interaction in **3**, which is consistent with Raman and IR features; the origins of which were attributed to both electronic differences in the equatorial coordination (i.e. inductive effects) and halogen polarizability (Br vs. I). Moreover, these results provide a starting point for characterization of interaction strengths via QTAIM, beginning with halogen-oxo interactions, based on the electron and energy densities found at interaction critical points, an effort that will complement energetics-based characterizations that are actively being applied to actinide hybrid materials.[9, 16, 51, 52]

Supporting Information Available

X-ray crystallographic files in CIF format, ORTEP figures of all compounds, PXRD spectra of all compounds, additional DFT data, solid-state luminescence spectra for compounds **3** and **4**, and tables of selected bond lengths are all available. CIFs have also been deposited at the Cambridge Crystallographic Database Centre and may be obtained from http://www.ccdc.cam.ac.uk by citing reference numbers 1838828-1838831 for compounds **1**-**4**, respectively.

Author Information

Corresponding Author

*E-mail: cahill@gwu.edu Phone: (202) 994-6959

Notes

The authors declare no competing financial interest.

Acknowledgement

This study was supported by the U.S. Department of Energy (DOE)—Chemical Sciences, Geosciences and Biosciences Division, Office of Basic Energy Sciences, Office of Science, Heavy Elements Program, under grant number DE-FG02-05ER15736. K. P. C. would also like to acknowledge The George Washington University for a Presidential Merit Fellowship award. The authors would also like to thank the Notre Dame University Energy Center for Infrared and Raman microscope time.

References

1. K.-X. Wang and J.-S. Chen, *Accounts of Chemical Research*, 2011, **44**, 531-540.
2. R. J. Baker, *Chemistry – A European Journal*, 2012, **18**, 16258-16271.
3. M. B. Andrews and C. L. Cahill, *Chemical Reviews*, 2013, **113**, 1121-1136.
4. R. E. Wilson, D. D. Schnaars, M. B. Andrews and C. L. Cahill, *Inorganic Chemistry*, 2014, **53**, 383-392.

5. L. Mei, C.-Z. Wang, L. Wang, Y.-L. Zhao, Z.-F. Chai and W.-Q. Shi, *Crystal Growth & Design*, 2015, **15**, 1395-1406.
6. R. G. Surbella III and C. L. Cahill, in *Handbook on the Physics and Chemistry of Rare Earths*, eds. J.-C. G. Bünzli and V. K. Pecharsky, Elsevier, Amsterdam, 2015, vol. 48, ch. 276, pp. 163-285.
7. P. Thuery and J. Harrowfield, *CrystEngComm*, 2016, **18**, 3905-3918.
8. M. Kalaj, K. P. Carter, A. V. Savchenkov, M. M. Pyrch and C. L. Cahill, *Inorganic Chemistry*, 2017, **56**, 9156-9168.
9. R. G. Surbella III, L. C. Ducati, K. L. Pellegrini, B. K. McNamara, J. Autschbach, J. M. Schwantes and C. L. Cahill, *Journal of the American Chemical Society*, 2017, **139**, 10843-10855.
10. K. P. Carter, A. T. Kerr, I. V. Taydakov and C. L. Cahill, *Solid State Sciences*, 2018, **76**, 20-32.
11. K. P. Carter, M. Kalaj, A. Kerridge, J. A. Ridenour and C. L. Cahill, *Inorganic Chemistry*, 2018, **57**, 2714-2723.
12. R. G. Surbella III, M. B. Andrews and C. L. Cahill, *Journal of Solid State Chemistry*, 2016, **236**, 257-271.
13. K. P. Carter and C. L. Cahill, *Inorganic Chemistry Frontiers*, 2015, **2**, 141-156.
14. K. P. Carter, M. Kalaj and C. L. Cahill, *Inorganic Chemistry Frontiers*, 2017, **4**, 65-78.
15. M. Kalaj, K. P. Carter and C. L. Cahill, *Acta Crystallographica Section B*, 2017, **73**, 234-239.
16. K. P. Carter, M. Kalaj, R. G. S. III, L. C. Ducati, J. Autschbach and C. L. Cahill, *Chemistry – A European Journal*, 2017, **23**, 15355-15369.
17. M. Kalaj, K. P. Carter and C. L. Cahill, *European Journal of Inorganic Chemistry*, 2017, **2017**, 4702-4713.
18. I. Dance, *New Journal of Chemistry*, 2003, **27**, 22-27.
19. H.-J. Schneider, *Angewandte Chemie International Edition*, 2009, **48**, 3924-3977.
20. M.-T. Nguyen, C. A. Pignedoli, M. Treier, R. Fasel and D. Passerone, *Physical Chemistry Chemical Physics*, 2010, **12**, 992-999.
21. S. Alvarez, *Dalton Transactions*, 2013, **42**, 8617-8636.
22. S. Fortier and T. W. Hayton, *Coordination Chemistry Reviews*, 2010, **254**, 197-214.
23. A. J. Lewis, H. Yin, P. J. Carroll and E. J. Schelter, *Dalton Transactions*, 2014, **43**, 10844-10851.
24. P. L. Arnold, A.-F. Pécharman, R. M. Lord, G. M. Jones, E. Hollis, G. S. Nichol, L. Maron, J. Fang, T. Davin and J. B. Love, *Inorganic Chemistry*, 2015, **54**, 3702-3710.
25. L. A. Seaman, E. A. Pedrick, G. Wu and T. W. Hayton, *Journal of Organometallic Chemistry*, 2018, **857**, 34-37.
26. N. L. Bell, B. Shaw, P. L. Arnold and J. B. Love, *Journal of the American Chemical Society*, 2018, **140**, 3378-3384.
27. J. de Groot, B. Cassell, M. Basile, T. Fetrow and T. Z. Forbes, *European Journal of Inorganic Chemistry*, 2017, **2017**, 1938-1946.
28. *SAINT*, Bruker AXS Inc., Madison, Wisconsin, USA, 2007.
29. *APEXII*, Bruker AXS Inc., Madison, Wisconsin, USA, 2008.

30. L. Krause, R. Herbst-Irmer, G. M. Sheldrick and D. Stalke, *Journal of Applied Crystallography*, 2015, **48**, 3-10.
31. *TWINABS*, Bruker AXS Inc., Madison, Wisconsin, USA, 2008.
32. A. Altomare, G. Cascarano, C. Giacovazzo, A. Guagliardi, M. C. Burla, G. Polidori and M. Camalli, *Journal of Applied Crystallography*, 1994, **27**, 435-435.
33. G. Sheldrick, *Acta Crystallographica Section A*, 2008, **64**, 112-122.
34. L. Farrugia, *Journal of Applied Crystallography*, 2012, **45**, 849-854.
35. CrystalMaker, *Journal*, 2009.
36. *JADE*, Materials Data Inc., Livermore, California, USA, 2003.
37. R. Ahlrichs, M. Bär, M. Häser, H. Horn and C. Kölmel, *Chemical Physics Letters*, 1989, **162**, 165-169.
38. F. Weigend and R. Ahlrichs, *Physical Chemistry Chemical Physics*, 2005, **7**, 3297-3305.
39. W. Küchle, M. Dolg, H. Stoll and H. Preuss, *The Journal of Chemical Physics*, 1994, **100**, 7535-7542.
40. P. Di Pietro and A. Kerridge, *Inorganic Chemistry*, 2016, **55**, 573-583.
41. P. Di Pietro and A. Kerridge, *Physical Chemistry Chemical Physics*, 2016, **18**, 16830-16839.
42. R. F. W. Bader, *Atoms in Molecules: A Quantum Theory*, Oxford University Press, Oxford, UK, 1990.
43. T. A. Keith, *AIMA11*, TK Gristmall Software, Overland Park, Kansas, USA, 2014.
44. A. Cousson, J. Proust, M. Pages, F. Robert and E. N. Rizkalla, *Acta Crystallographica Section C*, 1990, **46**, 2316-2318.
45. L. A. Watson and B. P. Hay, *Inorganic Chemistry*, 2011, **50**, 2599-2605.
46. C. Yige, Z. Weihai, S. Qingjin, Z. Weiping, Z. Jianshe, M. Jianyu, R. Zhanli and L. Chiyang, *Journal of Coordination Chemistry*, 2008, **61**, 3350-3356.
47. T. Loiseau, I. Mihalcea, N. Henry and C. Volkringer, *Coordination Chemistry Reviews*, 2014, **266–267**, 69-109.
48. G. Herzberg, *Infrared and Raman Spectra of Polyatomic Molecules*, D. Van Nostrand Company, Inc., New York, NY, 1946.
49. K. Nakamoto, *Infrared and Raman Spectra of Inorganic and Coordination Compounds Part A: Theory and Applications in Inorganic Chemistry*, John Wiley & Sons, Inc. , New York, NY, 5th edn., 1997.
50. L. H. Jones and R. A. Penneman, *The Journal of Chemical Physics*, 1953, **21**, 542-544.
51. C. Cannes, C. Le Naour, P. Moisy and P. Guilbaud, *Inorganic Chemistry*, 2013, **52**, 11218-11227.
52. N. Kumar and J. M. Seminario, *The Journal of Physical Chemistry C*, 2013, **117**, 24033-24041.